Check for updates

Analysis and detection of women's reproductive hormones using a bistable and reconfigurable 1D annular photonic crystal composed of the Ge₂Sb₂Te₅ phase-change material

Sakshi Gandhi and Suneet Kumar Awasthi [ID] *

In this study, the reconfigurable biosensing capabilities of the one-dimensional annular photonic structure, $(AB)^5CDC(AB)^5$, was examined theoretically. The proposed structure was made of concentric cylindrical layers of periodically modulated refractive indices, which were restricted in one direction only. Germanium antimony telluride (GST), which belongs to the class of phase-change materials (PCMs), was used in the fabrication of the proposed biosensing design. The entire study was carried out in the near-infrared region of the electromagnetic spectrum. The suggested biosensing structure was constructed by depositing alternate periodic cylindrical layers of SiO_2 and Si with a central air core. An air cavity coated on both sides by a phase-change chalcogenide material ($Ge_2Sb_2Te_5$) was introduced at the centre of the 1D annular photonic crystal to realize the $(AB)^5CDC(AB)^5$ structure. The simulation results of the proposed work were obtained using the MATLAB computational tool taking into consideration the modified transfer matrix method. The primary focus of this study was to measure the change in the position and intensity of the defect mode with respect to the change in the concentration levels of analytes containing progesterone and estradiol reproductive hormones separately in the amorphous and crystalline phases of the $Ge_2Sb_2Te_5$ material. Interestingly, a strong tunability in the position of the central wavelength of the defect mode inside the photonic band gap (PBG) was noticed during the phase transition of the GST material from amorphous to crystalline and back. In both the phases of the GST material, our design could identify minute refractive index variations in blood samples containing reproductive hormones at different concentrations for monitoring various gynaecological disorders in women. Besides sensitivity, other important parameters such as the limit of detection, signal-to-noise ratio, and quality factor were estimated to evaluate the biosensing capabilities of the proposed design.

1. Introduction

Hormones are one of the most important chemical messengers used for transporting messages between different body organs so that these organs may execute relevant activities for the functioning of the human body.[1,2] A minute imbalance in the hormone levels can cause severe disorders inside the body including tumours, osteoporosis, and cardiac dysfunction. Therefore, periodically monitoring the hormone levels is a highly essential requirement to avoid disorders, which can develop in the human body due to an imbalance in the hormone levels.[3,4] The human body contains a variety of hormones, which are deliberately used for transporting signals to different body organs so that they can execute the desirable work. In the present study, we focused our attention towards the

progesterone and estradiol reproductive hormones in both males and females. These reproductive hormones play significant roles during puberty, fertility, and sexuality throughout the human life.[5] Actually, reproductive hormones are created in the ovaries and testes of females and males, respectively. The progesterone and estrogen hormones are essential for reproductive growth and signify the sexual health of an individual. These hormones are equally important in both males and females and are responsible for the production of eggs in females.[6,7] The estrogen hormone influences several internal activities in the human body including the thickening of the uterine lining in females to make it ready for the probable implantation of a fertilized egg cell. A female body releases more estrogen hormones as compared to male bodies. They are also responsible for maintaining the cholesterol level. Additionally, estrogen hormones are responsible for the prevention of osteoporosis by strengthening the bones in both men and women. During the reproductive period, the most frequent form of estrogen hormone in females is estradiol.

Department of Physics and Material Science and Engineering, Jaypee Institute of Information Technology, Noida 201304, U.P., India. E-mail: suneet_electronic@yahoo.com

Disproportionality of the estradiol hormone in both females and males may lead to certain diseases, including depression and skin problems in addition to osteoporosis, which may result in fractures in the bones. A high level of the estradiol hormone may become the root cause of uterine and breast cancer in females as well as gynaecomastia disease in males.[8,9] A low level of estradiol may lead to the development of obesity and cardiovascular problems. On the other hand, progesterone hormones make a significant contribution during pregnancy by decreasing the uterine contractility through the development of the mammary gland.[10,11] The interaction between these hormones is accountable for the changes that appear in the body during the pregnancy period. Moreover, progesterone is also involved in various internal activities such as blood pressure regulation and the control of mood swings and also helps during relaxation and sleep. In several methods of contraception, the pairing of estrogen with progesterone is used to suppress fertilization. Therefore, there is an essential requirement to monitor the levels of both these reproductive hormones, especially in the female body, to maintain their balance in the reproductive system for the evaluation of the overall health.[12]

From the beginning of the previous century, the importance of maintaining hormone levels in the human body was recognized, and consequently considerable significant research work associated with different kinds of innovative biosensors capable of detecting the concentrations of various hormone levels in the human body have been developed. Most of the biosensors that are being used by biomedical professionals are based on immunometric assay approaches for the accurate identification and detection of the concentration levels of various hormones in the body. Nonetheless, biosensors based on immunometric assay approaches have several disadvantages, including time efficiency, low sensitivity, accuracy rate, and selectivity.[13–16] Besides, traditional pathological investigation requires experienced laboratory staff and well-equipped laboratories to conduct specific pathological tests for identifying the levels of particular hormones in the human body.[17,18] The currently available photonic biosensing technology may provide a solution to these technological challenges in a better way.

The past few decades have witnessed the emergence of photonic crystals (PhCs) as a promising candidate to design and develop various optical devices with a tremendous ability to control and manipulate the flow of electromagnetic waves (EMWs) passing through them.[19] PhCs are engineered multi-layer periodic structures in which the periodic arrangement of the constituent material layers is in one, two, or three dimensions of space. Based on the periodic arrangement of the constituent layers, PhCs can be classified into one-dimensional (1D), two-dimensional (2D), or three-dimensional (3D).[20] The fabrication of 1D PhCs is very simple and cost effective in contrast to 2D and 3D PhCs, which attracted the attention of researchers working in the field of photonic engineering to make cost-effective photonic products to reach common people. Actually PhCs have a tremendous capability for controlling and manipulating electromagnetic waves because they possess photonic band gaps (PBGs).[21,22] The ranges of frequencies of

incident electromagnetic radiation which lies inside PBGs are not permitted to travel into the structure except for the radiation of frequencies which lies outside.[23] A break in the periodicity of photonic structures can lead to the existence of a defect mode with high transmittance inside the PBG of the structure due to photon confinement inside the cavity region. The width of the PBG and the defect mode position inside the PBG are strongly affected by changes in the structural variables, like in the refractive index of the materials used, the thickness of distinct layers, and the incident angle, period number, and nature of the polarization of incident light. The PBG characteristics of 1D photonic structures are also responsible for affecting the reflection, absorption, and transmittance properties of the structure. It is thought that the PBG-dependent optical properties of photonic structures may be used to improve the working of a wide range of optical devices, such as biosensors, photodetectors, lasers, solar cells, optical switches, and photonic waveguides.[24–26] Additionally, the biosensing abilities of annular photonic crystals (APCs) have also attracted the attention of researchers worldwide for the development of highly efficient photonic biosensing structures due to the efficiency, rapidity, accuracy, and sensitivity found in the results of biosensors composed of APCs. Such APCs are made up of concentric and periodic cylindrical layers whose refractive index variation is restricted only in one direction.[27,28] Moreover, the necessity of examining the levels of reproductive hormones has attracted us towards the development of a 1D APC-based biosensor with the special ability to sense and detect the reproductive hormone levels in both males and females. These hormones are also known as sex hormones and can be easily examined through the blood or urine samples of the patient. Nowadays, a wide range of photonic biosensing technology-based biosensors are available for the effective investigation of the biological and chemical properties of the samples under consideration. These samples are termed as analytes. For example, Hussein et al. theoretically explored the temperature-detection abilities of a 1D defective annular photonic crystal (DAPC). They used a modified transfer matrix method approach based on a cylindrical coordinate system.[29–31] Arafa et al., on the other hand, proposed how a 1D APC could be utilized efficiently as an effective air purifier in the ultraviolet (UV) region of the electromagnetic spectrum for minimizing the possibility of spreading airborne communicable diseases, like COVID-19.[32] Moreover, Abadla et al. suggested a highly efficient Tamm/Fano resonance-based 1D APC biosensor capable of identifying the refractive index fluctuations of biofluids ranging from 1 to 1.5.[33] The aforementioned biosensing capabilities of 1D APC-based structures have attracted the attention of researchers globally for designing different types of biosensors as a low cost and efficient alternative compared to conventional biosensing designs.

The above-mentioned piece of remarkable research work motivated us to explore a way by which a 1D defective annular photonic structure could be used as a bi-stable and reconfigurable biosensor for the effective detection of the reproductive hormone levels in the human body.[34–40] Another reason behind this motivation was to examine the bi-stable and reconfigurable

behaviour of the 1D defective annular photonic structure with GST-coated cavity walls similar to the work of Arafa *et al.*, who conducted a study on 1D planar photonic structures for the detection of the reproductive hormones *via* the blood samples of women.[41,42] The working principle of our proposed annular photonic structure is based on the detection of a small change in the refractive index of a blood sample containing reproductive hormones of different concentrations present in the sample under consideration. To the best of our knowledge, such a kind of bi-stable and reconfigurable biosensing device composed of 1D defective APC with GST-coated cavity walls for the detection of the estradiol and progesterone hormone levels present in a blood sample has not been investigated to date. This manuscript is organized as follows. Section 1 presents the introduction to the proposed work. The design specifications are discussed in Section 2. Theoretical formulations pertaining to the work are given in Section 3. Section 4 deals with the results and discussions pertaining to the work. Finally, Section 5 of this manuscript presents the conclusion of the work.

2. Description of the proposed design

The architecture of the proposed photonic biosensing device $(AB)^N CDC(AB)^N$ is shown in Fig. 1. This device consisted of a 1D defective APC with coated cavity walls. The letters A and B represent the periodic and coaxial cylindrical layers of silicon (Si) and silicon dioxide (SiO_2) of the design, respectively.[41] The cylindrical cavity layer D of air was surrounded on both sides by the phase-change material (PCM) layer C,[42] as shown in Fig. 1. The purpose of using identical coaxial cylindrical layers of the germanium antimony telluride (GST) material with $Ge_2Sb_2Te_5$ on either side of an air cavity layer was to protect the Si layer of the structure from direct exposure to air and to the water content present in the sample. Moreover, the involvement of the
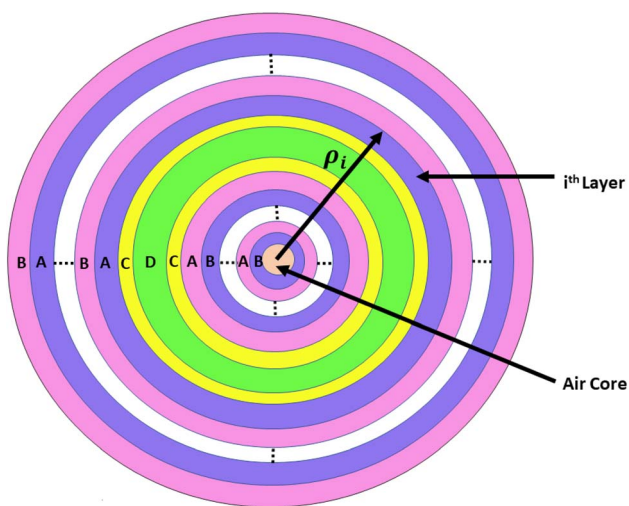

Fig. 1 Top view of the proposed biosensing structure made up of concentric cylindrical layers with an air core. Here, the letters A, B, C, and D represent cylindrical layers of Si, SiO_2, GST, and air, respectively. The symbol ρ_i is used to represent the radial distance of the *i*th cylindrical layer from the axis of the proposed biosensor.

GST brings the additional features of bi-stability and reconfigurability into our design. Actually, GST belongs to a class of PCM that can be easily switched to amorphous and crystalline phases by applying either electrical or optical or thermal energy on the GST material layers by an appropriate amount. We used the letter N to denote the period number of the proposed structure. The thickness of the coaxial cylindrical layers A, B, C, and D were denoted by d_1, d_2, d_3, and d_D, respectively. The notations n_1 and n_2 represent the refractive indexes of layers A and B made up of Si and SiO_2, respectively. The air cavity region D of the proposed work was used to infiltrate the cavity region with the sample under consideration. The refractive indices of the GST material $Ge_2Sb_2Te_5$ under amorphous and crystalline phases were represented by n_a and n_c, respectively. The refractive indices of the samples containing estradiol and progesterone hormones separately were being represented by the letters n_e and n_p, respectively, which were dependent upon their concentration.

For experimental realization of the proposed work, we used a wide-band light source at the axis of the annular photonic structure in addition to a single mode fibre and direction couplers. The blood sample circulation chamber was installed near the top of the cavity layer with the facility of IN and OUT ports. These ports were utilized for sample loading and extraction. A shift in the position of the defect mode due to changes in the concentration levels of different reproductive hormones present in the blood sample inside the PBG could be easily analyzed on the computer screen with the help of an optical spectrum analyzer and interfacing software. Moreover, we had to comply with all the well-known sets of rules and regulations for the preparation of reproductive hormones of different concentration levels extracted from human blood as one of the mandatory requirements for obtaining the desired level of accuracy from the results biosensors.

The optimum thicknesses of the concentric and periodic coaxial cylindrical layers A, B, C, and D were chosen as $d_1 = 390$ nm, $d_2 = 180$ nm, $d_3 = 50$ nm, and $d_D = 1150$ nm, respectively. The refractive indices of layers A and B were taken as 3.3 and 1.45, respectively, in the near-infrared region of the electromagnetic spectrum. The period number N was fixed as 5.

3. Theoretical formulation of the proposed biosensor

This section elaborates the modified transfer matrix method in the cylindrical coordinate system. This method describes the interaction between the proposed structure composed of 1D defective APC and the incident electromagnetic waves propagating radially outward from the axis of the proposed structure, as shown in Fig. 1. The structure was periodic only along the radial direction and infinitely extended along the z direction.

The unit cell of the periodic part of the proposed design consisted of the cylindrical layers A and B, as shown in Fig. 1. The refractive indices and thicknesses of the A and B layers were denoted as n_1 and n_2 and d_1 and d_2, respectively. The radial

distance of the ith cylindrical layer from the axis of the 1D defective APC is as described in ref. [43–45] and as below:

$$\rho_i = \begin{cases} \rho_\text{o} + \dfrac{i-1}{2}\Delta + d_1 & i = 1,3,5,\ldots 2N-1 \\[2mm] \rho_0 + \dfrac{i}{2}\Delta & i == 0,2,4,\ldots 2N \end{cases} \tag{1}$$

where N represents the period number of the proposed bilayer periodic structure composed of defective APC $(AB)^5 CDC (AB)^5$. Here, the notations $i = 1, 3, 5,\ldots 2N-1$ and $i = 0, 2, 4,\ldots 2N$ are used to represent odd and even interfaces of the ith layer of the structure. For cylindrical kinds of Bragg waves, two configurations of wave propagation corresponding to the TE and TM modes are possible. This work deals only with propagation of cylindrical Bragg waves corresponding to the TE mode only. The modified transfer matrix method used to connect the electric and magnetic fields at the forward and backward interface of the ith cylindrical layer of the refractive index n_i of the defective APC structure in a cylindrical coordinate system is defined as in ref. [43–45] and as below:

$$\begin{bmatrix} V(\rho_i) \\ U(\rho_i) \end{bmatrix} = \begin{bmatrix} X_i(1,1) & X_i(1,2) \\ X_i(2,1) & X_i(2,2) \end{bmatrix} \begin{bmatrix} V(\rho_{i-1}) \\ U(\rho_{i-1}) \end{bmatrix} \tag{2}$$

The elements of the matrix X_i are described as

$$X_i(1,1) = \frac{\pi}{2} k_i \rho_{i-1} \left[Y'_m(k_i \rho_{i-1}) J_m(k_i \rho_i) - J'_m(k_i \rho_{i-1}) Y_m(k_i i) \right] \tag{3a}$$

$$X_i(1,2) = j\frac{\pi}{2} \frac{k_i}{p_i} \rho_{i-1} [J_m(k_i \rho_{i-1}) Y_m(k_i \rho_i) - Y_m(k_i \rho_{i-1}) J_m(k_i \rho_i)] \tag{3b}$$

$$X_i(2,1) = -j\frac{\pi}{2} k_i \rho_{i-1} p_i \left[Y'_m(k_i \rho_{i-1}) J'_m(k_i \rho_i) - J'_m(k_i \rho_{i-1}) Y'_m(k_i \rho_i) \right] \tag{3c}$$

$$X_i(2,2) = \frac{\pi}{2} k_i \rho_{i-1} \left[J_m(k_i \rho_{i-1}) Y'_m(k_i \rho_i) - Y_m(k_i \rho_{i-1}) J'_m(k_i \rho_i) \right] \tag{3d}$$

The resultant transfer matrix Z connecting the first to last interfaces of all the cylindrical layers used in the formation of the proposed defective APC structure $(AB)^5 CDC (AB)^5$ can be established as

$$\begin{bmatrix} V(\rho_\text{f}) \\ U(\rho_\text{f}) \end{bmatrix} = Z \begin{bmatrix} V(\rho_i) \\ U(\rho_i) \end{bmatrix} \tag{4}$$

where $Z = Z_{2N} Z_{2N-1}\ldots Z_2 Z_1 Z_\text{C} Z_\text{D} Z_\text{C} Z_1 Z_2 \ldots Z_{2N-1} Z_{2N}$.

The transmission coefficient of the proposed 1D defective APC structure can be obtained as

$$t = \frac{4}{\pi \rho_0 H_m^{\ 1}(k_0 \rho_0) H_m^{\ 2}(k_0 \rho_0)} \\ \times \frac{1}{\left[\left(jp_0 S_{m0}^{(1)} Z - Z_{21} \right) - jp_\text{f} S_\text{mf}^{(2)} \left(-jp_0 S_{m0}^{(1)} Z_{12} - Z_{22} \right) \right]} \tag{5}$$

where Z_{11}, Z_{12}, Z_{21}, and Z_{22} are the elements of the 2×2 matrix Z representing the transfer matrix of the entire structure. The notations p_o and p_f are used for denoting the admittances of the core and the last medium of the structure, respectively. We used the subscripts o and f to represent the incident and exit media of the design, respectively. The admittance is defined as

$$P_i = \sqrt{\frac{\varepsilon_i}{\mu_i}} \quad (i = o \text{ and } f) \tag{6}$$

where ε_i and μ_i denote the electric permittivity and magnetic permeability of any ith cylindrical layer of the structure. The notations o and f represent the core (incident medium) and substrate (exit medium) layers, respectively, of the structure. The equation for S_{mi} is defined as

$$S_{mi}^{(1,2)} = \frac{H'^{(1,2)}_m(k_i \rho_i)}{H^{(1,2)}_m(k_i \rho_i)} \tag{7}$$

The Hankel functions of the first and second kind are denoted as the notations $H_m^{(1)}$ and $H_m^{(2)}$, respectively. Here, the notations are representing their respective derivatives.

The transmittance of the proposed photonic biosensing device is obtained from ref. [43–45] and is given by the equation below.

$$T = tt^* = |t|^2 \tag{8}$$

4. Results and discussion

In this section, the results and discussions of the proposed biosensing design composed of the defective APC are presented. This device was capable of identifying the concentration levels of progesterone and estradiol reproductive hormones present in samples. Before discussing the results pertaining to the work, first the significance of reproductive hormones along with the concentration-dependent refractive index values of blood samples containing progesterone and estradiol reproductive hormones are discussed in Section 3.1.

4.1 Significance of the reproductive hormones progesterone and estradiol, along with their concentration-dependent refractive index values, in blood samples

The evaluation of progesterone hormones in females is an important measure during the early stages of pregnancy as well as in cases of irregular menstruation. The progesterone hormone is largely responsible for the ovulation process, which releases the mature eggs from the ovary to the fallopian tube. It is a cyclic process through which women have to pass every month.[8–11] During this period, the eggs released by a woman's body are ready to combine with a man's sperm, which is responsible for fertilization. An excess release of the progesterone hormone may disturb the biological process of fertilization in females. Furthermore, estradiol is another reproductive hormone that plays a significant role in assuring

the growth, maintenance, and development of reproductive organs in addition to mammary glands, uterine tubes, and the vagina throughout puberty, youth, and pregnancy. An insufficient amount of the estradiol hormone may also become a root cause of osteoporosis, which inhibits the growth, progress, and development of bones in the human body. Aside from that, one of the key functions of the estradiol hormone is normalization of a recurring interval of sexual receptivity.[12]

The complex refractive index of GST under amorphous and crystalline phases was defined in eqn (9) and (10), respectively. Experimentally determined complex refractive index values of GST under amorphous and crystalline phases were used to establish the theoretical relations in eqn (11)–(14), representing the wavelength-dependent real and imaginary parts of the complex refractive index values of GST under amorphous and crystalline phases. Polynomial curve fitting of degrees 4 and 5 were utilized to ensure a greater accuracy and precision between the theoretical and experimental findings.

$$na = naGST + iKaGST \qquad (9)$$

$$nc = ncGST + iKcGST \qquad (10)$$

Here, the notations naGST and kaGST represent the real and imaginary components of the complex refractive index of GST under the amorphous phase. The curve fitting formulas showing the wavelength-dependent real and imaginary parts of the complex refractive index of GST under the amorphous phase are given as

$$naGST = -0.51929\lambda^4 + 4.3531\lambda^3 - 12.984\lambda^2 + 15.789\lambda - 2.0315 \qquad (11)$$

$$KaGST = -0.29346\lambda^3 + 2.3145\lambda^2 - 5.9547\lambda + 4.9925 \qquad (12)$$

Similarly, a curve fitting formula can also be applied to obtain the wavelength-dependent real and imaginary parts of the complex refractive index of GST under the crystalline phase, as given in eqn (13) and (14), respectively, below

$$ncGST = 1.2751\lambda^3 - 8.1973\lambda^2 + 16.168\lambda - 2.9464 \qquad (13)$$

$$KcGST = -0.72443\lambda^4 + 5.461\lambda^3 - 13.331\lambda^2 + 9.7612\lambda + 1.8907 \qquad (14)$$

Additionally, in the near-infrared region, GST reflects a significant contrast between the complex refractive index values under the amorphous and crystalline phases. The capability of a change in the refractive index values of GST under the amorphous and crystalline phases offers a novel pathway towards developing tuneable and reconfigurable photonic biosensors with extremely high sensitivity.

Next, we defined eqn (15) and (16) for determining the refractive index of blood samples containing progesterone and estradiol reproductive hormones, respectively, at different concentrations.[39,40] These relations were determined by using cubic curve fitting applied on an experimentally observed refractive index of values of blood samples containing progesterone and estradiol hormones of different concentrations.

$$n_p = 4.2882 \times 10^{-8}c^3 + 2.2847 \times 10^{-6}c^2 + 4.5962 \times 10^{-5}c + 1.3352 \qquad (15)$$

$$n_e = 2.678 \times 10^{-4}c^3 + 1.7648 \times 10^{-3}c^2 + 3.7489 \times 10^{-3}c + 1.3333 \qquad (16)$$

Here, c is used to represent the level of concentration of progesterone and estradiol hormones present in the analyte, measured in nmol L^{-1}. The distinct refractive index values of blood samples containing progesterone and estradiol hormones of different concentration present in the samples was obtained from eqn (15) and (16), respectively. These values are listed in Table 1 below.

4.2 Modulation in the defect mode position of the proposed biosensor loaded with water samples corresponding to the amorphous and crystalline phases of Ge₂Sb₂Te₅

Here, we present the working principles of the proposed biosensing device composed of defective APC. For this purpose, the cavity region of the structure was infiltrated with water sample with a refractive index of 1.333, and we investigated the transmission properties of the proposed 1D biophotonic sensor $(AB)^5CDC(AB)^5$, whose cavity walls were coated with the PCM made up of GST, in order to make our proposed biosensing design bi-stable and reconfigurable. The phase of the Ge₂Sb₂Te₅ could be switched between the crystalline and amorphous states by applying optical or electrical or thermal energy in an appropriate amount at the coaxial cylindrical layers made up of GST, *i.e.* the layer represented by the letter C, as previously defined. The coherent approach based on the modified transfer matrix method (MTMM) and MATLAB computational software was applied to extract the results for this work. The transmission spectrum of the proposed biosensor $(AB)^5CDC(AB)^5$ under the crystalline phase of GST loaded with a water sample was plotted in Fig. 2(a), where it can be seen that there existed a single defect mode of transmittance close to unity, which was located at the wavelength of 2220 nm inside the PBG, extending from 2100 nm to 2350 nm.

Table 1 Distinct refractive index values of analytes containing the reproductive hormones progesterone and estradiol at different levels of concentration

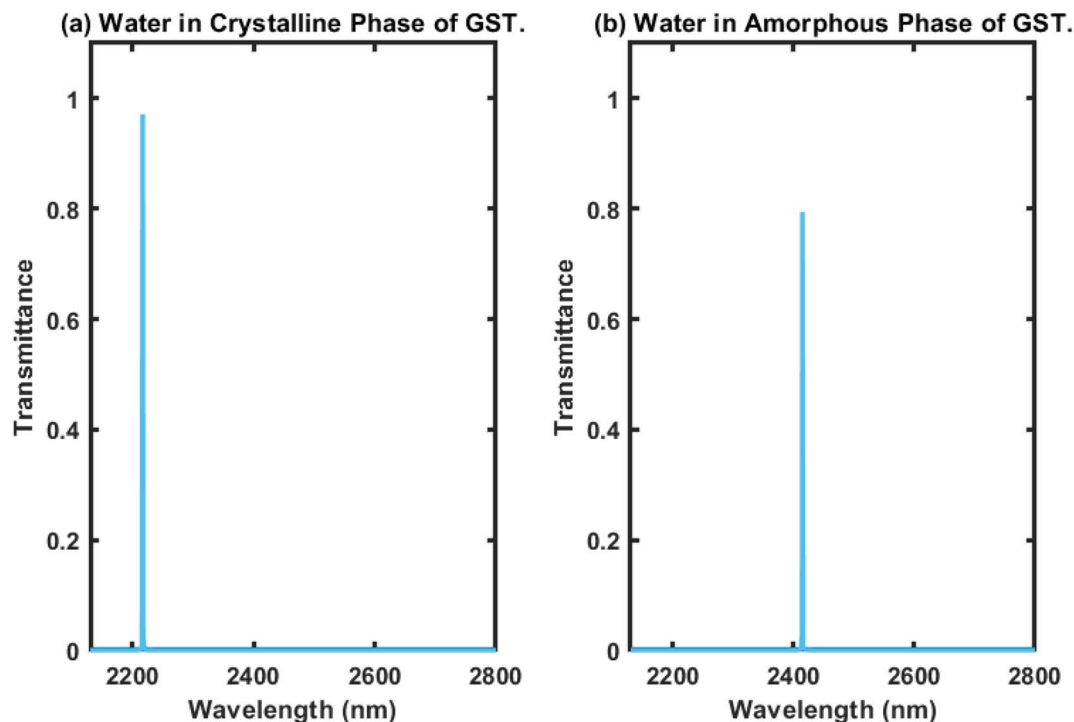| Reproductive hormones			
Progesterone		Estradiol	
Concentration (nmol L^{-1})	Refractive index	Concentration (nmol L^{-1})	Refractive index
0	1.3352	0	1.3333
40	1.3361	5	1.3413
80	1.3462	7	1.3647
120	1.3819	9	1.4190
160	1.4596	11	1.5170
200	1.5961		

Fig. 2 Transmittance of the proposed 1D photonic biosensor composed of 1D defective APC infiltrated with a water sample of cavity thickness $d_D = 1150$ nm under the influence of (a) the crystalline phase and (b) amorphous phase of $Ge_2Sb_2Te_5$.

The transmittance of the suggested design under identical circumstances as elaborated above in the amorphous phase of $Ge_2Sb_2Te_5$ was plotted and the results are shown in Fig. 2(b). This shows that as we switched the phase of $Ge_2Sb_2Te_5$ from crystalline to amorphous, the central wavelength of the defect mode earlier located at a wavelength of 2220 nm was relocated to a new position at a wavelength of 2420 nm. Additionally, this change in phase of GST also advanced the PBG to a new position between 2300 nm to 2550 nm, as shown in Fig. 2(b). The transmittance of the defect mode under the amorphous phase of GST inside the PBG located at 2420 nm was reduced by 80% due to the increase in the imaginary part of the complex index of refraction of $Ge_2Sb_2Te_5$ when in the amorphous phase. In both cases, the full width at half maximum (FWHM) was narrow, which is an essential requirement for the design of any high-performance biosensors. Thus, it can be concluded that the PCM-based APCs can be employed for the fabrication of reconfigurable, bi-stable, and tuneable photonic biosensors.

4.3 Effect of changes in the concentration level of progesterone reproductive hormones present in the blood samples under investigation on the transmittance of the proposed biosensor under the crystalline and amorphous phases of $Ge_2Sb_2Te_5$

In this section, we first examine the transmittance of the proposed biophotonic sensor $(AB)^5CDC(AB)^5$ loaded with blood samples (analytes) containing progesterone hormone at different concentration levels, 0, 40, 80, 120, 160, and 200 nmol L^{-1}, separately, under the crystalline phase of $Ge_2Sb_2Te_5$. The

transmittance plot showing the six defect modes marked by the colours blue, red, yellow, purple, green, and light blue, corresponding to analytes containing progesterone reproductive hormone at concentration levels of 0, 40, 80, 120, 160, and 200 nmol L^{-1}, respectively, inside PBG ranging from 2200 nm to 2350 nm are presented in Fig. 3(a) under the influence of the crystalline phase of the GST material. It could be seen that as the concentration changed from 0 nmol L^{-1} to 200 nmol L^{-1}, according to data present in Table 1, the respective defect modes started to shift towards the higher wavelength side in addition to the PBG. Moreover their intensity gradually decreased and nearly reached 80% when the cavity was loaded with a blood sample containing progesterone hormone at 200 nmol L^{-1}. This reduction in intensity was due to the increase in the molecules of progesterone hormones present in the sample, which resulted in more scattering of light inside the cavity. This reduction in the intensity associated with a defect mode inside PBG could easily be seen using an optical spectrum analyzer (Ocean Optics spectrometer USB4000).

Next, efforts were made to examine the behaviour of the proposed photonic biosensing design when its cavity was loaded separately with blood samples containing progesterone hormone at different concentration levels under the influence of the amorphous phase of $Ge_2Sb_2Te_5$. This study was conducted to verify our claim that the proposed structure can be used as a bi-stable and reconfigurable photonic biosensor. For this purpose, the cavity region of the proposed 1D photonic biosensor $(AB)^5CDC(AB)^5$ composed of 1D defective APC was infiltrated with blood samples containing progesterone
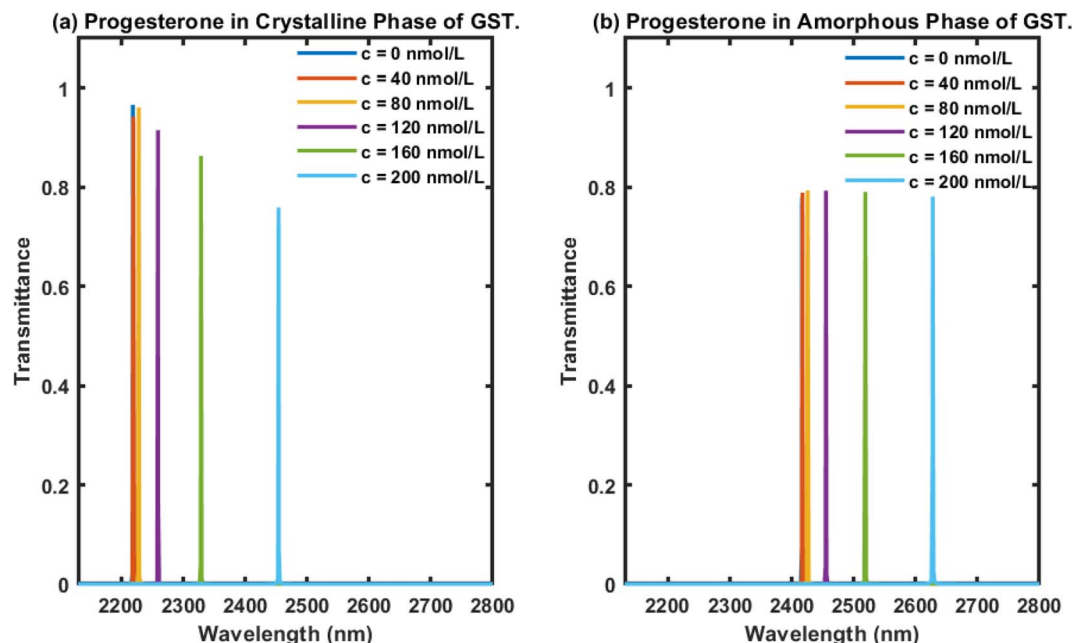
Fig. 3 Transmittance of the proposed 1D photonic biosensing design composed of 1D defective APC infiltrated with analytes containing progesterone hormones at different concentration levels as 0, 40, 80, 120, 160, and 200 nmol L^{-1}, separately, inside a cavity of thickness $d_D = 1150$ nm under the influence of the (a) crystalline phase and (b) amorphous phase of Ge$_2$Sb$_2$Te$_5$. The transmittance plot shows six distinguishable defect modes coloured here blue, red, yellow, purple, green, and light blue corresponding to analytes containing reproductive hormone progesterone at 0, 40, 80, 120, 160, and 200 nmol L^{-1}, respectively.

hormone at concentrations of 0, 40, 80, 120, 160, and 200 nmol L^{-1}, separately, under the amorphous phase of GST. The transmittance of the proposed biosensor loaded with analytes containing progesterone hormone at concentrations of 0, 40, 80, 120, 160, and 200 nmol L^{-1} are plotted in Fig. 3(b). This shows six distinguishable defect modes coloured here blue, red, yellow, purple, green, and light blue corresponding to blood samples containing progesterone hormones at concentrations of 0, 40, 80, 120, 160, and 200 nmol L^{-1}, respectively, inside the PBG ranging from 2400 nm to 2650 nm. It is evident from Fig. 3(b) that the increase in the concentration of progesterone present in the analyte was responsible for the movement of the PBG and the respective defect modes located inside the PBG towards the higher wavelength side. Surprisingly, we also noted that all the defect modes had almost identical intensities located inside the PBG, ranging from 2400 nm to 2650 nm. The intensities of the defect modes were close to 80%, which would be more than enough to be detected by an optical spectrum analyzer used. The variation in the intensity of defect modes associated with the different samples under investigation is one of the major drawbacks involved with the structures used for photonic biosensing applications. Comparisons among the results in Fig. 3 showed that the use of Ge$_2$Sb$_2$Te$_5$ in the amorphous phase overcome the drawbacks of the intensity variation associated with the defect modes of the proposed structure loaded with different samples with the crystalline phase of GST. This study may also provide an insight to promote the use of GST in the amorphous phase in the design of biophotonic sensors to overcome the drawbacks of the intensity

variations that occur in the defect modes of photonic biosensors loaded with different samples.

4.4 Effect of changes in the concentration level of estradiol reproductive hormones present in the blood samples under investigation on the transmittance of the proposed biosensor when tested under the crystalline and amorphous phases of Ge$_2$Sb$_2$Te$_5$

Next, we examined the behaviour of the proposed biophotonic sensor (AB)^{5}CDC(AB)^5 loaded with blood samples containing estradiol hormones at concentrations of 0, 5, 7, 9 and 11 nmol L^{-1}, separately, under the influence of both the crystalline and amorphous phases of Ge$_2$Sb$_2$Te$_5$. The thickness of the cavity was chosen as $d_D = 1150$ nm. The respective transmittance plots of the proposed biosensor under the influence of both the crystalline and amorphous phases of Ge$_2$Sb$_2$Te$_5$ are shown in Fig. 4(a) and (b), respectively. Fig. 4 shows five defect modes coloured here blue, red, yellow, purple, and green, corresponding to analytes containing estradiol hormones at concentrations of 0, 5, 7, 9, and 11 nmol L^{-1}, respectively. The central wavelength of the defect modes present inside the PBG of the design under the influence of both phases of GST was modulated towards the higher wavelength side as the concentration of estradiol hormone in the samples increased (Fig. 4). Additionally, it could be noticed in Fig. 4(a) that under the crystalline phase of GST, our design displayed a reduction in the intensity of the defect mode associated with the higher concentration samples, and this reduction was sufficient enough to be easily detected by an Ocean Optics spectrometer, USB4000.
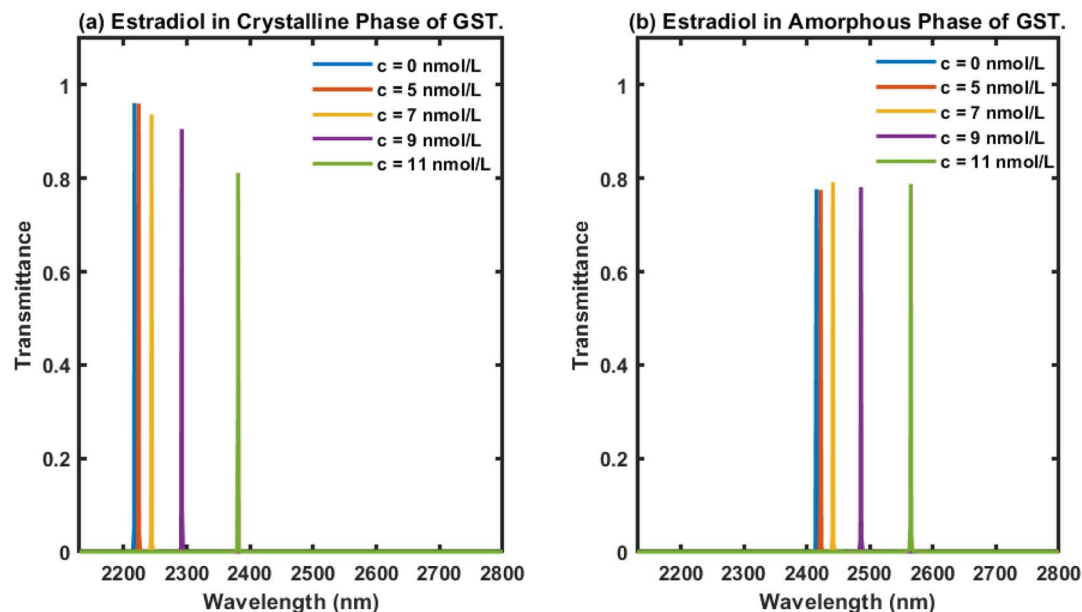
Fig. 4 Transmittance plots of the proposed 1D photonic biosensing design composed of 1D defective APC infiltrated with analytes containing estradiol hormones at different concentrations as 0, 5, 7, 9, and 11 nmol L^{-1}, separately, inside a cavity of thickness $d_D = 1150$ nm under the influence of the (a) crystalline phase and (b) amorphous phase of $Ge_2Sb_2Te_5$. The transmission spectra showed five defect modes coloured blue, red, yellow, purple, and green in the figure, corresponding to analytes containing estradiol hormone at concentrations of 0, 5, 7, 9, and 11 nmol L^{-1}, respectively.

Finally, we turned our attention to examining the behaviour of the proposed design loaded with analytes containing estradiol hormones at different concentrations of 0, 5, 7, 9, and 11 nmol L^{-1}, separately, under the influence of the amorphous phase of $Ge_2Sb_2Te_5$ and a cavity thickness d_D of 1150 nm. The transmittance of the proposed biosensor loaded with analytes containing estradiol hormones at the aforementioned concentration levels was plotted and the results are shown in Fig. 4(b). As can be seen in Fig. 4(b), five defect modes were distinguishable, here coloured blue, red, yellow, purple, and green, corresponding to analytes containing estradiol hormones at different concentrations of 0, 5, 7, 9, and 11 nmol L^{-1}, respectively, inside the PBG extending from 2375 nm to 2640 nm. This also reflected that as the concentration of estradiol present in the analyte under investigation increased, the central wavelength of the respective defect modes inside the PBG ranging from 2375 nm to 2640 nm moved towards the higher wavelength side. This behaviour was similar to the results in Fig. 3. All five defect modes inside the PBG of the design originated due to the infiltration of the cavity of the structure with analytes containing estradiol hormones at concentrations of 0, 5, 7, 9, and 11 nmol L^{-1}, separately. All these defect modes had an identical intensity of 80%, as evident in Fig. 4(b). The energy associated with each defect mode would be more than sufficient to meet the threshold value of the detector for accurate sensing and detection.

The comparison between the nature of transmittance of the proposed 1D defective APC-based biosensing design $(AB)^5CD$-$C(AB)^5$ infiltrated with blood samples containing progesterone and estradiol hormones of various concentration levels under the influence of the crystalline and amorphous phases of $Ge_2Sb_2Te_5$ as shown in Fig. 3 and 4, respectively, illustrated the bistable and reconfigurable behaviour of the proposed biosensor. Moreover, these results were also reflected in the FWHM of each defect mode of the structure loaded with both types of blood samples containing progesterone and estradiol hormones being smaller in the case with the crystalline phase of $Ge_2Sb_2Te_5$. A small FWHM is always an essential requirement for the design of sensitive photonic biosensing devices. Our study successfully demonstrated that under both phases of $Ge_2Sb_2Te_5$ the proposed 1D defective APC-based photonic biosensor $(AB)^5CDC(AB)^5$ was capable of identifying minute changes in the refractive index of different blood samples containing progesterone and estradiol hormones of various concentration levels. The infiltration of various blood samples did not cause any significant reduction in the intensity of the defect modes, which makes our design suitable to be used for the accurate sensing and detection of reproductive hormones under the influence of both the crystalline and amorphous phases of $Ge_2Sb_2Te_5$. The involvement of the phase-change material (PCM) in the fabrication of the structure makes our design bistable and reconfigurable.

4.5 Analysis of the working performance of the proposed biosensor

In order to examine the working performance of our suggested 1D photonic biosensing design composed of 1D defective APC, we evaluated the sensitivity (S), figure of merit (FoM), limit of detection (LoD), quality factor (Q), and signal-to-noise ratio (SnR) performances of our design. These are the most

important and significant parameters in the analysis of biosensors based on photonic, plasmonic, and photonic crystal fibre technologies. The sensitivity is the most important of all the parameters as it determines the change in position of the central wavelength of the defect mode peak ($\Delta\lambda$) within the PBG due to any change in the refractive index of the blood samples (Δn) under consideration. A high sensitivity value is always needed for the design of any high-performing photonic biosensors. It is given by eqn (17),

$$S = \frac{\Delta\lambda}{\Delta n}\,(\text{nm per RIU}) \qquad (17)$$

The parameter Q indicates how effectively a biosensor can work, and indicates how small a change in the refractive index of a sample could still be precisely and accurately sensed by any biosensor. For quality biosensing applications, a high value of Q is always preferred. It is defined as,

$$Q = \frac{\lambda_{\text{defect}}}{\text{FWHM}} \qquad (18)$$

The parameter FoM is directly proportional to the sensitivity of any biosensing device and is inversely proportional to the FWHM of the defect mode inside the PBG. For any biosensor to work efficiently, a large FoM value is always required. The FoM is defined as,

$$\text{FOM} = \frac{S}{\text{FWHM}} \qquad (19)$$

Besides the above parameters, two more parameters, namely the SnR and LoD, were also investigated to appraise the effective working of the proposed biosensor, as defined mathematically in eqn (20) and (21), respectively.

$$\text{SnR} = \frac{\Delta\lambda}{\text{FWHM}} \qquad (20)$$

and

$$\text{LoD} = \frac{3}{2}\frac{\text{FWHM}}{S(\text{SnR})^{1/4}} \qquad (21)$$

Based on the parameters described above in eqn (17)–(21), we evaluated the performance of our suggested 1D defective APC-based photonic biosensing design $(AB)^5CDC(AB)^5$ with coated cavity walls loaded with analytes containing progesterone and estradiol of different concentration levels under the crystalline and amorphous phases of $Ge_2Sb_2Te_5$. The numerical values of S, Q, FoM, LoD, and SnR were calculated from eqn (17)–(21), respectively, and are summarized in Tables 2 and 3 for when the structure was loaded with analytes containing progesterone and estradiol at different concentration levels under the crystalline phase of $Ge_2Sb_2Te_5$, respectively.

In all this work, we used the optimized value of the cavity layer as $d_D = 1150$ nm. To determine this optimum value, we measured the sensitivity of the design loaded with blood samples containing reproductive hormones of different concentrations with varying d_D thicknesses of 650, 750, 850, 950, 1050, 1150, and 1250 nm, separately. This process helped us to estimate the optimum value of the cavity layer thickness. For example, we present a plot of the sensitivity *versus* cavity layer thickness of the proposed structure loaded with a blood sample containing estradiol hormone at 7 nmol L^{-1} under the influence of the amorphous phase of GST in Fig. 5. This figure shows that the sensitivity of the proposed design reached

Table 2 Different performance–evaluation parameters of the proposed biosensing design $(AB)^5CDC(AB)^5$ infiltrated with analytes containing progesterone hormones at different concentration levels of 0, 40, 80, 120, 160, and 200 nmol L^{-1} with the crystalline phase of $Ge_2Sb_2Te_5$

c (nmol L^{-1})	Refractive index (RIU)	Wavelength (nm)	FWHM (nm)	Sensitivity (nm nmol^{-1} L^{-1})	Quality factor	FoM (nmol L^{-1})	LoD	SnR
0	1.3352	2218	0.180		12 322.22		0.009	
40	1.3361	2219	0.225	1111.11	9862.22	4938.27	1.013×10^{-5}	4.44
80	1.3462	2228	0.225	909.09	9902.22	4040.40	1.238×10^{-5}	44.44
120	1.3819	2259	0.225	877.94	10 040.00	3901.97	1.281×10^{-5}	182.22
160	1.4597	2329	0.225	891.59	10 351.11	3962.52	1.262×10^{-5}	493.33
200	1.5951	2454	0.180	908.04	13 633.33	5044.68	9.91×10^{-6}	1311.11

Table 3 Different performance–evaluation parameters of the proposed biosensing design $(AB)^5CDC(AB)^5$ infiltrated with analytes containing progesterone hormones at different concentration levels of 0, 40, 80, 120, 160, and 200 nmol L^{-1} with the amorphous phase of $Ge_2Sb_2Te_5$

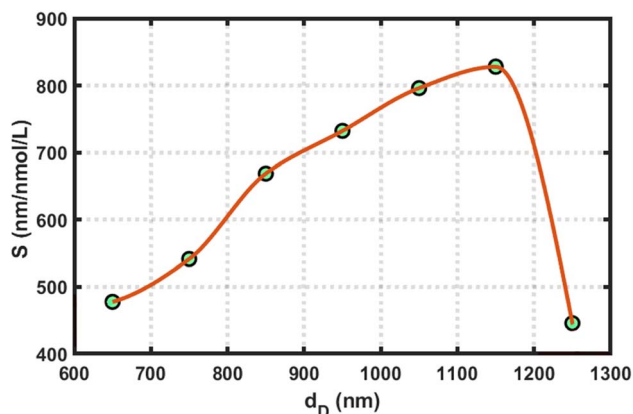| c (nmol L^{-1})	Refractive index (RIU)	Wavelength (nm)	FWHM (nm)	Sensitivity (nm nmol^{-1} L^{-1})	Quality factor	FoM (nmol L^{-1})	LoD	SnR
0	1.3352	2416	0.225		10 737.78		0.01125	
40	1.3361	2417	0.315	1111.11	7673.02	3527.34	1.418×10^{-5}	3.17
80	1.3462	2426	0.315	909.09	7701.59	2886.00	1.733×10^{-5}	31.75
120	1.3819	2455	0.27	835.12	9092.60	3093.03	1.617×10^{-5}	144.44
160	1.4597	2519	0.315	839.45	7996.83	2664.91	1.876×10^{-5}	326.98
200	1.5951	2628	0.495	1111.11	5309.09	2241.67	2.228×10^{-5}	428.28

Fig. 5 Sensitivity *versus* cavity layer thickness variations of the proposed structure loaded with a blood sample containing estradiol hormone at 7 nmol L^{-1} under the amorphous phase of GST.

a maximum value of 828.03 nmol L^{-1}, corresponding to d_{D} = 1150 nm. Further increases in the cavity layer thickness affected the sensitivity of the proposed APC structure; therefore, our choice of selecting the optimum value of cavity layer thickness as d_{D} = 1150 nm in this work is justified.

The numerical values of S, Q, FoM, LoD, and SnR of the proposed biosensor loaded with analytes containing progesterone hormone at different concentrations of 0, 40, 80, 120, 160, and 200 nmol L^{-1} under the crystalline phase of Ge$_2$Sb$_2$Te$_5$ are listed in Table 2. It can be seen in the table that the sensitivity of the design varied between 877.94 nm nmol^{-1} L^{-1}, corresponding to the blood sample containing progesterone hormones at 120 nmol L^{-1}, and 1111.11 nm nmol^{-1} L^{-1}, corresponding to the sample with a concentration of 40 nm nmol^{-1} L^{-1}. The maximum achieved value of the FoM of the proposed biosensor was 5044.68 nmol L^{-1}. This value was high, as expected. The lowest achieved LoD value was 9.91 × 10^{-6}. The SnR values of the proposed design varied between 4.44 and 1311.11.

Next, we examined the performance of the proposed structure loaded with analytes containing progesterone hormones at concentration levels of 0, 40, 80, 120, 160, and 200 nmol L^{-1} under the amorphous phase of Ge$_2$Sb$_2$Te$_5$ by evaluating the parameters S, Q, FoM, LoD, and SnR as mentioned above with the help of eqn (17)–(21), respectively. The data are listed in Table 3 below. Comparison of the data presented in Table 2 with Table 3 shows that under the influence of the amorphous phase of Ge$_2$Sb$_2$Te$_5$, the performance of the proposed structure loaded with progesterone hormones at the different concentration levels was marginally compromised due to the increase in the imaginary part of the complex refractive index of Ge$_2$Sb$_2$Te$_5$ when in the amorphous phase in comparison to in the crystalline phase. These observations are similar to the findings of Arafa *et al.*[41]

Next, linear curve fitting was applied on the data in Tables 2 and 3 to observe the behaviour of the changes in the position of the defect mode corresponding to blood samples containing progesterone hormones at different concentration levels under the influence of the crystalline and amorphous phase of GST, respectively. This linear curve fitting yielded two empirical relations, eqn (22) and (23), which gave straight line plots, as shown in Fig. 6(a) and (b), corresponding to the crystalline and amorphous phases of GST, respectively. The empirical relations eqn (22) and (23) as defined below are plotted in Fig. 6(a) and (b), respectively. The straight lines plotted in Fig. 6 gave slopes of 892.16 and 815.03, which indicated respective sensitivities of 892.16 nm per RIU and 815.03 nm per RIU under the crystalline and amorphous phases of GST. It is clear from the slopes from eqn (22) and (23) that the structure was more sensitive for observing changes in the refractive index of the sample containing progesterone hormones at different concentrations under the crystalline phase of GST as compared to the amorphous phase.

$$(\lambda_{\mathrm{D}}^{\mathrm{p}})_{\mathrm{Cry}} = 906.52 n_{\mathrm{p}} + 1007.2 \tag{22}$$

$$(\lambda_{\mathrm{D}}^{\mathrm{p}})_{\mathrm{Amo}} = 815.03 n_{\mathrm{p}} + 1328.4 \tag{23}$$
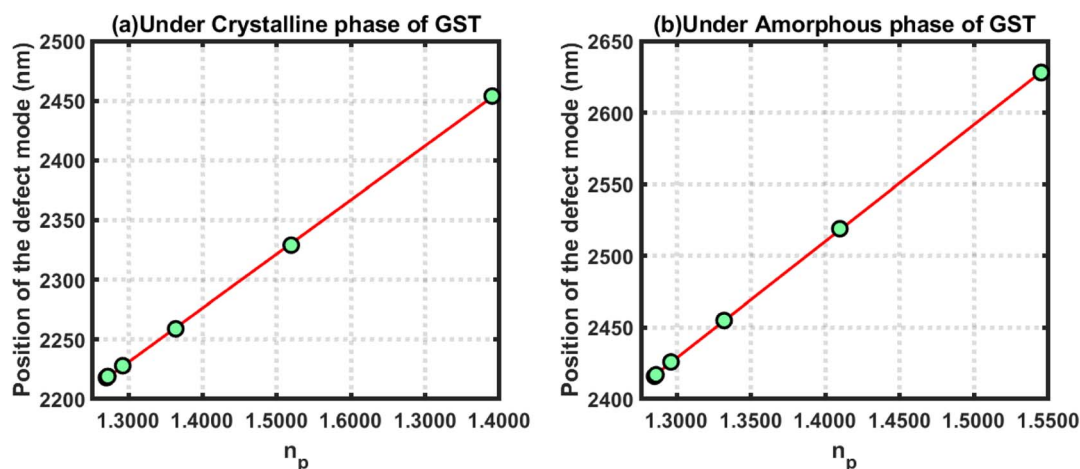

Fig. 6 Defect mode position *versus* refractive index of blood samples containing progesterone hormones at different concentration levels under the influence of the (a) crystalline and (b) amorphous phase of GST.

where $(\lambda_D^p)_{Cry}$ and $(\lambda_D^p)_{Amo}$ represent the positions of the defect mode under the influence of the crystalline and amorphous phases of GST, respectively.

Further, we evaluated the performance of our proposed design loaded with estradiol hormones of various concentration levels under the influence of the crystalline phase of $Ge_2Sb_2Te_5$. The numeric values of S, Q, FoM, LoD, and SnR of the proposed design loaded with blood samples containing estradiol hormones at concentrations of 0, 5, 7, 9, and 11 nmol L^{-1} under the influence of the crystalline phase of $Ge_2Sb_2Te_5$ are listed in Table 4.

The above-mentioned performance–evaluation parameters of the proposed structure loaded with blood samples containing estradiol hormones at different concentration levels under the amorphous phase of $Ge_2Sb_2Te_5$ are listed in Table 5. Again, we noticed that the sensing performance of the proposed structure loaded with blood samples containing estradiol hormones at different concentration was little bit compromised in the amorphous phase of $Ge_2Sb_2Te_5$ in comparison to the crystalline phase.

Further, efforts were made to study the behaviour of the changes in the position of the defect mode due to changes in the refractive index of blood samples containing estradiol hormones at various concentration levels under the crystalline and amorphous phase of GST by applying linear curve fitting on the data in Tables 4 and 5, respectively, as discussed above. The linear curve fitting yielded two empirical relations that govern the movement of the defect mode inside the PBG of the proposed structure loaded with blood samples containing estradiol hormones at different concentration levels, as described below in eqn (24) and (25), under the influence of the crystalline and amorphous phases of GST, respectively.

$$(\lambda_D^e)_{Cry} = 892.16 n_e + 1027 \qquad (24)$$

$$(\lambda_D^e)_{Amo} = 815.39 n_e + 1328.3 \qquad (25)$$

where $(\lambda_D^e)_{Cry}$ and $(\lambda_D^e)_{Amo}$ represent the positions of the defect mode under the influence of the crystalline and amorphous phases of GST, respectively.

The above empirical relations are plotted in Fig. 7 below, which shows straight lines corresponding to the crystalline and amorphous phases of GST. The slopes of the lines plotted in Fig. 7(a) and (b) were 892.16 and 815.39, respectively. This yield that the sensitivities of the structure loaded with blood samples containing estradiol under the crystalline and amorphous phase were 892.16 nm per RIU and 815.39 nm per RIU, respectively. Additionally, the structure was more sensitive under the crystalline phase as compared to the amorphous phase. In both cases, the sensitivity reached an ultrahigh level compared to the results reported in ref. [41] and [42].

It can be clearly seen from the data presented in Tables 2 and 4 that under the influence of the crystalline phase of $Ge_2Sb_2Te_5$ loaded with blood containing progesterone and estradiol hormones at different concentration levels separately, the sensing abilities of the proposed design were significantly enhanced as compared to the sensing abilities of the structure under the amorphous phase of $Ge_2Sb_2Te_5$. Moreover, the sensing ability of the structure under both phases of $Ge_2Sb_2Te_5$ was sufficient for the minute and accurate detection of reproductive hormones at different concentrations present in the samples. Additionally, the involvement of GST makes our 1D defective APC structure a bi-stable and reconfigurable biosensor.

Thus our design can be used for the sensing and detection of blood samples containing reproductive hormones at different concentration levels under the crystalline and amorphous phases of $Ge_2Sb_2Te_5$. GST can be a preferable choice for the design and development of 1D defective annular photonic

Table 4 Different performance–evaluation parameters of the proposed biosensing design $(AB)^5CDC(AB)^5$ infiltrated with analytes containing estradiol hormones at different concentration levels of 0, 5, 7, 9, and 11 nmol L^{-1} under the crystalline phase of $Ge_2Sb_2Te_5$

c (nmol L^{-1})	Refractive index (RIU)	Wavelength (nm)	FWHM (nm)	Sensitivity (nm nmol^{-1} L)	Quality factor	FoM (nmol L^{-1})	LoD	SnR
0	1.3330	2217	0.315		7038.09		0.01575	
5	1.3413	2224	0.270	873.80	8237.04	3236.29	1.545×10^{-5}	25.93
7	1.3647	2244	0.315	858.52	7123.81	2725.46	1.835×10^{-5}	85.71
9	1.4190	2292	0.270	874.81	8488.89	3240.03	1.543×10^{-5}	272.78
11	1.5170	2381	0.315	892.68	7558.73	2833.90	1.764×10^{-5}	520.63

Table 5 Different performance–evaluation parameters of the proposed biosensing design $(AB)^5CDC(AB)^5$ infiltrated with analytes containing estradiol hormones at different concentration levels of 0, 5, 7, 9, and 11 nmol L^{-1} under the amorphous phase of $Ge_2Sb_2Te_5$

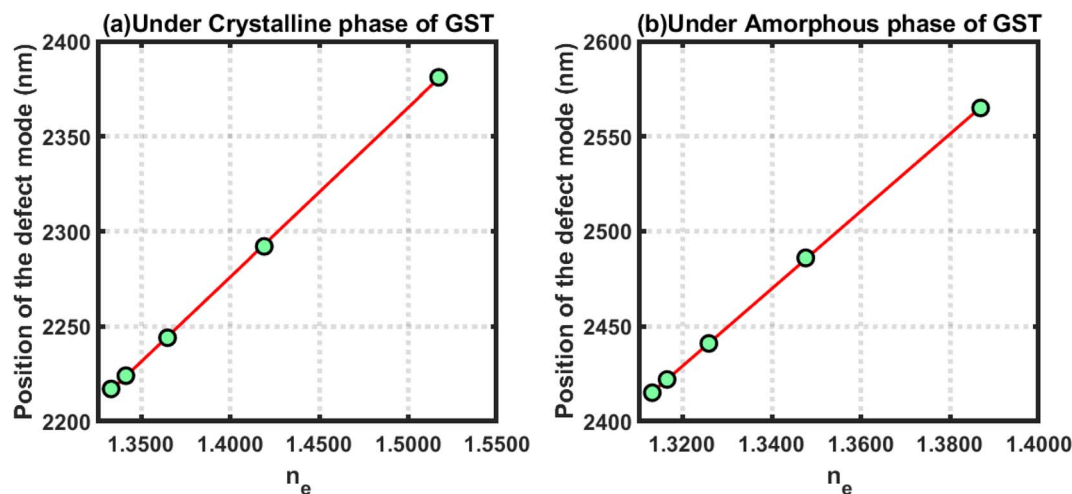| c (nmol L^{-1})	Refractive index (RIU)	Wavelength (nm)	FWHM (nm)	Sensitivity (nm nmol^{-1} L)	Quality factor	FoM (nmol L^{-1})	LoD	SnR
0	1.3330	2415	0.315		7666.67		0.01575	
5	1.3413	2422	0.360	875.00	6727.78	2430.56	2.057×10^{-5}	19.44
7	1.3647	2441	0.315	828.03	7749.21	2628.65	1.902×10^{-5}	82.54
9	1.4190	2486	0.315	828.47	7892.06	2630.07	1.901×10^{-5}	222.22
11	1.5170	2565	0.450	816.55	5700.00	1814.55	2.756×10^{-5}	333.33

Fig. 7 Defect mode position verses refractive index of blood samples containing estradiol hormones at different concentration levels under the influence of the (a) crystalline and (b) amorphous phases of GST.

structure-based biosensing devices for the detection of minute changes in the refractive index of samples under consideration. Furthermore, an inbuilt switching property between the crystalline and amorphous phases of GST can open a new gateway for the development of APC-based externally tuneable bio-photonic devices.

Finally, before concluding this work, we present a quick comparison between the proposed work and the earlier works of distinguished researchers based on photonic biosensing technology. This comparison shows that the APC structures can be better choice for designing various biosensors over planar photonic crystals. The proposed design has a higher sensitivity,

Table 6 Comparison highlighting the sensitivity, quality factor, and FoM values of the proposed design in contrast to the earlier works of other photonic workers

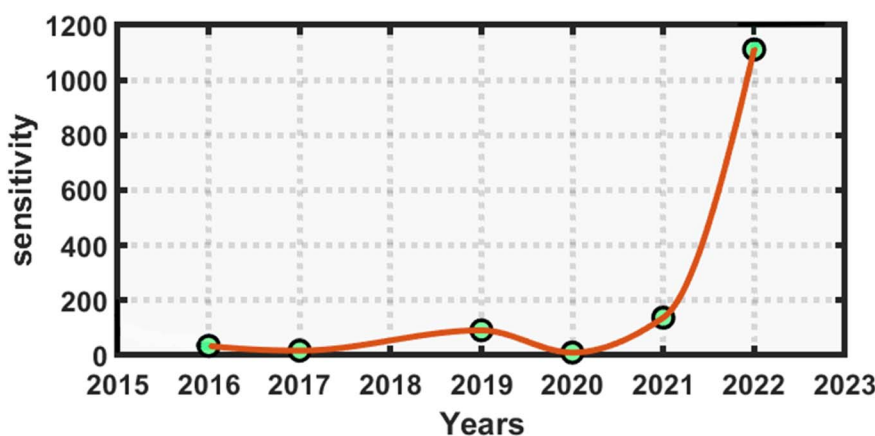| Year	S (nm per RIU)	Q factor	FoM	Frequency range	Ref.
2016	34.11	—	1.1×10^3	THz	46
2017	17	3×10^4	2.23×10^2	Visible to NIR	47
2019	53.0–90.9	—	—	NIR	48
2020	10	3×10^2	15.1	Visible	49
2021	137.02–30.44	$(0.12–1.43) \times 10^4$	$(0.2–2.7) \times 10^3$	Visible	41
2021	55.55–98.92	$(0.68–2.3) \times 10^4$	$(1.96–2.6) \times 10^4$	Visible	42
This work	816.54–1111.11	$(0.57–1.36) \times 10^4$	$(0.22–0.5) \times 10^4$	NIR	

Fig. 8 Annual statistical data comparing the performance of the proposed annular photonic biosensor with earlier designed biosensors in terms of the reported sensitivity.

ranging from 816 to 1111.11 nm nmol^{-1} L^{-1}, which represents an ultrahigh sensitivity compared to similar kinds of biosensing work based on planar photonic structures for the detection of reproductive hormones.[41,42] The orders of the Q factor and FoM values of our design were either equal or higher compared to those in previous works given in Table 6 below. This shows that the suggested biosensor had a reasonably higher sensitivity and much better performance compared to similar kinds of sensors in other research works for the detection of reproductive hormones in females. Fig. 8 below presents the statistical requirements of our work in terms of sensitivity in comparison to the similar kinds of photonic biosensing works presented in Table 6.

5. Conclusion

In this work, we theoretically investigated the biosensing properties of the proposed 1D defective APC-based photonic biosensor composed of GST with the help of a modified transfer matrix method and MATLAB simulation software. The performance of the proposed structure loaded with blood samples containing progesterone and estradiol hormones at different concentration levels were separately evaluated in both the crystalline and amorphous phases of Ge$_2$Sb$_2$Te$_5$. The application of GST in the fabrication of the proposed structure makes our design bi-stable and reconfigurable due to the ability of the coexistence of the dual phases of Ge$_2$Sb$_2$Te$_5$, *i.e.* crystalline and amorphous. In both the states corresponding to the crystalline and amorphous phases of Ge$_2$Sb$_2$Te$_5$, the sensitivity variation of the proposed structure was between 816.54 and 1111.11 nm nmol^{-1} L^{-1}, which is very high. This value of sensitivity is ultrahigh compared to the sensitivities achieved in planar photonic biosensing designs proposed by other researchers. This analysis shows that the application of GST under its amorphous phase may be used to overcome the drawback of intensity variations associated with the defect modes of proposed structures loaded with different samples under the crystalline phase of GST. This property may provide an insight to promote the use of GST in its amorphous phase in the design of biophotonic sensors with defect modes of uniform intensity inside the PBG associated with various biosamples under investigation.

Data availability

The results of the present theoretical work are based on MATLAB simulations. All the relations and other relevant information have been properly cited throughout the manuscript keeping the ease of readers of the journal. The readers can easily reproduce the results of the work with the help of theoretical details given in the manuscript and MATLAB computational software.

Conflicts of interest

The authors do not have any conflicts of interest.

References

1 A. B. Hodsman, D. C. Bauer, D. W. Dempster, L. Dian, D. A. Hanley, S. T. Harris, D. L. Kendler, M. R. McClung, P. D. Miller, W. P. Olszynski, E. Orwoll and C. K. Yuen, *Endocr. Rev.*, 2005, **26**, 688–703, DOI: **10.1210/er.2004-0006**.

2 E. Hagstrom, P. Hellman, T. E. Larsson, E. Ingelsson, L. Berglund, J. Sundstrom, H. Melhus, C. Held, L. Lind, K. Michaelsson and J. Arnlov, *Circulation*, 2009, **119**, 2765–2771, DOI: **10.1161/CIRCULATIONAHA.108.808733**.

3 B. Zafrani, M. H. Aubriot, E. Mouret, P. De Cremoux, Y. De Rycke, A. Nicolas, E. Boudou, A. Vincent-Salomon, H. Magdelenat and X. Satre-Garau, *Histopathology*, 2000, **37**, 536–545, DOI: **10.1046/j.1365-2559.2000.01006.x**.

4 S. M. Hsu, L. Raine and H. Fanger, *Am. J. Clin. Pathol.*, 2016, **75**, 734–738, DOI: **10.1093/ajcp/75.5.734**.

5 **https://slidetodoc.com/reproductive-hormones-reproductive-hormones-male-gonads-testes-produce/**.

6 E. Zeidan, R. Shivaji, V. C. Henrich and M. G. Sandros, *Sci. Rep.*, 2016, **6**, 26714, DOI: **10.1038/srep26714**.

7 A. Lieberman and L. Curtis, *Altern. Ther. Health Med.*, 2017, **23**(7), 14–22.

8 J. C. Prior, *Drug Discovery Today: Dis. Models*, 2020, **32**(B), 31–40, DOI: **10.1016/j.ddmod.2020.11.005**.

9 F. J. Demayo, B. Zhao, N. Takamoto and S. Y. Tsai, *Ann. N. Y. Acad. Sci.*, 2002, **955**, 48–59, DOI: **10.1111/j.1749-6632.2002.tb02765.x**.

10 **https://my.clevelandclinic.org/health/treatments/15245-hormone-therapy-for-menopause-symptoms**.

11 **https://www.medicalnewstoday.com/articles/277177#types**.

12 N. Ramanujam, A. Panda, P. Yupapin, A. Natesan and P. Prabpal, *Phys. B*, 2022, **639**, 414011, DOI: **10.1016/j.physb.2022.414011**.

13 A. H. Aly, Z. A. Zaky, A. S. Shalaby, A. M. Ahmed and D. Vigneswaran, *Phys. Scr.*, 2020, **95**, 35510–35516, DOI: **10.1088/1402-4896/ab53f5**.

14 A. Panda, P. P. Devi and G. Keiser, in *2019 International Workshop on Fiber Optics in Access Networks, (FOAN)*, 2019, pp. 23–25, DOI: **10.1109/FOAN.2019.8933813**.

15 Z. A. Zaky and A. H. Aly, *J. Supercond. Novel Magn.*, 2020, **33**, 2983–2990.

16 N. R. Ramanujam, J. El-KhozondarHala, D. Vigneswaran, T. Sofyan and A. H. Aly, *Phys. B*, 2019, **572**, 42–55, DOI: **10.016/j.physb.2019.07.051**.

17 A. Panda and P. P. Devi, *Opt. Quantum Electron.*, 2021, **53**, 357, DOI: **10.1007/s11082-021-03012-9**.

18 O. Soltani, J. Zaghdoudi and M. Kanzari, *Photonics Nanostruct.*, 2020, **38**, 100744, DOI: **10.1016/j.photonics.2019.100744**.

19 A. H. Aly, S. K. Awasthi, D. Mohamed, Z. S. Matar, M. Al-Dossari and A. F. Amin, *RSC Adv.*, 2021, **11**, 32973.

20 S. K. Awasthi, U. Malaviya and S. P. Ojha, *J. Opt. Soc. Am. B*, 2006, **23**, 2566–2571.

21 S. K. Awasthi, U. Malaviya and S. P. Ojha, *J. Nanophotonics*, 2008, **2**, 023505.

22 S. K. Awasthi, R. Panda and L. Shiveshwari, *Phys. Plasmas*, 2017, **24**(7), 072111.

23 S. K. Awasthi, A. Mishra, U. Malaviya and S. P. Ojha, *Solid State Commun.*, 2009, **149**(33–34), 1379.

24 Z. A. Zaky and A. H. Aly, *Sci. Rep.*, 2021, **11**, 1–9.

25 S. Gao, Y. Dou, Q. Li and X. Jiang, *Opt. Express*, 2017, **25**, 7112–7120.

26 B. Suthar and A. Bhargava, *Silicon*, 2020, **13**, 1765–1768.

27 H. Kurt and D. S. Citrin, *Opt. Express*, 2005, **25**, 10316–10326, DOI: **10.1364/OPEX.13.010316**.

28 S. Gandhi, S. K. Awasthi and A. H. Aly, *RSC Adv.*, 2011, **11**, 26655–26665, DOI: **10.1039/D1RA04166E**.

29 M. M. Abadla, H. A. Elsayed and A. Mehaney, *Physica E*, 2020, **119**, 114020, DOI: **10.1016/j.physe.2020.114020**.

30 M. M. Abadla, H. A. Elsayed and A. Mehaney, *Phys. Scr.*, 2020, **95**, 085508, DOI: **10.1088/1402-4896/aba2b0**.

31 M. M. Abadla, H. A. Elsayed and A. Mehaney, *Nature*, 2020, **13**, 4737–4745, DOI: **10.1007/s12633-020-00788-5**.

32 A. A. Ameen, H. A. ElSayed and A. H. Aly, *RSC Adv.*, 2021, **11**, 14915, DOI: **10.1039/d1ra00991e**.

33 A. Mehaney, M. M. Abadla and H. A. Elsayed, *J. Mol. Liq.*, 2021, **322**, 114978, DOI: **10.1016/j.molliq.2020.114978**.

34 M. Kaliteevski, I. Iorsh, S. Brand, R. Abram, J. Chamberlain and A. Kavokin, *Phys. Rev. B*, 2007, **76**, 165415–165468.

35 J. A. Gaspar-Armenta and F. Villa, *J. Opt. Soc. Am. B*, 2003, **20**, 2349–2354.

36 M. Makaraviciute and A. Ramanavicius, *Anal. Methods*, 2015, **7**, 9875–9884.

37 N. German and A. Kausaite-Minkstimiene, *Analyst*, 2013, **138**, 1427–1433.

38 G. Pitruzzello and T. F. Karuss, *J. Opt.*, 2018, **20**, 073004.

39 S. E. Abd El-Ghany, W. M. Noum, Z. Matar, Z. A. Zaky and A. H. Aly, *Phys. Scr.*, 2020, **96**, 035501.

40 S. Sudro, F. Carpignano, L. M. Strambini, S. Merlo and G. Barillaro, *RSC Adv.*, 2014, **4**, 51935–51941.

41 A. H. Aly, S. K. Awasthi, A. Mohamed, M. Al-Dossari, Z. Matar, M. Mohaseb, N. El-Gawaad and A. Amin, *Phys. Scr.*, 2021, **96**, 125533, DOI: **10.1088/1402-4896/ac3efa**.

42 A. H. Aly, S. K. Awasthi, A. M. Mohamed, Z. S. Matar, M. A. Mohaseb, M. Al-Dossari, M. T. Tammam, Z. A. Zaky, A. F. Amin and W. Sabra, *Crystals*, 2021, **11**, 1533, DOI: **10.3390/cryst11121533**.

43 V. A. Pedrosa, J. Yan, A. L. Simonian and A. Revzin, *Electroanalysis*, 2011, **23**, 1142–1149, DOI: **10.1002/elan.201000654**.

44 S. Pineda, Z. J. Han and K. Ostrikov, *Materials*, 2014, **7**, 4896–4929, DOI: **10.3390/ma7074896**.

45 Z. Chen, M. Lu, D. Zou and H. Wang, *J. Environ. Sci.*, 2012, **24**, 541–549, DOI: **10.1016/S1001-0742(11)60722-5**.

46 A. Purkayastha, T. Srivastava and R. Jha, *Sens. Actuators B*, 2016, **227**, 291–295.

47 V. V. Klimov, A. A. Pavlov, I. V. Treshin and I. V. Zabkov, *J. Phys. D: Appl. Phys.*, 2017, **50**, 285101.

48 N. R. Ramanujam, H. A. El-Khozondar, V. Dhasarathan, S. A. Tayae and A. H. Aly, *Phys. B*, 2019, **572**, 42–55.

49 G. Lheureux, M. Monavarian, R. Anderson, R. A. DeCrescent, J. Bellessa, C. Synmonds, J. A. Schuller, J. Speck, S. Nakamura and S. P. DenBaars, *Opt. Express*, 2020, **28**, 17934–17943.